

Delaminated Zeolites: Combining the Benefits of Zeolites and Mesoporous Materials for Catalytic Uses

A. Corma,¹ V. Fornés, J. Martínez-Triguero, and S. B. Pergher

Instituto de Tecnología Química (UPV-CSIC), Universidad Politécnica de Valencia, Avda. de los Naranjos, s/n, 46022 Valencia, Spain

Received November 26, 1998; revised February 5, 1999; accepted March 23, 1999

The delamination of the layered precursor of the MCM-22 zeolite (MWW structure) affords monolayers of a crystalline aluminosilicate with more than $700 \text{ m}^2 \text{ g}^{-1}$ of a well defined external surface formed by cups of $0.7 \times 0.7 \text{ nm}$. In this layered structure the circular 10-member-ring microporous system is preserved. The resultant material presents the strong acidity and stability characteristic of the zeolites but, at the same time, offers the high accessibility to large molecules characteristic of the amorphous aluminosilicates. The cracking behavior during the process of small and large molecules has been compared with that of the zeolite MCM-22 and pillared laminar precursor MCM-36. © 1999 Academic Press

INTRODUCTION

Since the first catalytic studies carried out in the 1960s on faujasite and mordenite zeolites, the possibilities of these materials have been greatly expanded due to the synthesis of many new structures containing pores with 8, 10, and 12 member rings (MR) whose diameters range between 0.4 and 0.75 nm. With the wide spectrum of structures presently available, it is possible, in many cases, to find an existing structure which matches the size of the pore with the size of the reactant molecule or, even better, with the size of the transition state of the reaction (1). Synthesis efforts are directed nowadays toward the understanding of the mechanisms of nucleation and crystal growing and the role played by the structure directing agent (SDA), with the aim of achieving synthesis by design (2–7). However, until this is reached, the synthesis of new structures continues to be based on accumulated knowledge, good common sense, and a little serendipity.

Recently, new zeolitic materials, which combine in the same structure pores with different diameters, have been synthesized with the hope of achieving new selectivity effects that cannot be expected on zeolite topologies formed by a single system of pores (1). Thus, structures containing simultaneously 10- and 12-MR pores which either cross (SSZ-26, Nu-87) (2, 8), are independent (MWW type) (9),

or even combine 10-, 11-, and 12-MR pores (Nu-86) (10) have been synthesized. However, and to the best of our knowledge, these topologies have not up to now shown unique and characteristic catalytic selectivity.

In the synthesis of new zeolite structures it is of continuous interest to find molecular sieve materials with large and ultralarge pores that can be active in catalytic reactions involving large reactant molecules or products. In this sense, they may have a positive impact on important processes such as fluid catalytic cracking (FCC) or hydrocracking or even in the production of chemicals and fine chemicals. Some success in this direction has been attained recently with the discovery of unidirectional 14MR zeolites such as UTD-1 (11) and CIT-5 (12). Despite the initial expectation for these zeolites, it has been found (13) that they do not represent a clear advantage with respect to the tridirectional 12MR USY and Beta zeolites for the cracking of vacuum gasoil.

The search for zeolites, which render the active sites more accessible to bulky molecules, has led to the modification of their textural properties by postchemical treatments designed to generate mesopores, as occurs in the cases of USY(14) and modified mordenite (15), or to synthesize small zeolite crystals (16) that show a high ratio of external to internal surface. There is no doubt that the external surface of zeolites retains geometrical and chemical characteristics of the bulk structure and can participate actively in catalytic processes (17, 18). Thus, it can be highly desirable to prepare zeolitic materials with well-defined, large external surface areas, which still present some of the characteristic confinement of the microporous materials.

This idea has been specifically applied in the case of the MWW-type materials, whose structure grows by layers and it is possible to obtain a zeolite precursor in which the layers are still not condensed (19). At this point, if one allows the layers to condense, the MWW structure is obtained, and this is composed of two independent pore systems: one is formed by 12-MR cages ($1.8 \times 0.7 \text{ nm}$) connected by 10-MR apertures, and the other one is defined by a well differentiated 10-MR circular channel (Fig. 1) (9). This type of microporous structure is not only inaccessible to large

¹ To whom correspondence should be addressed.

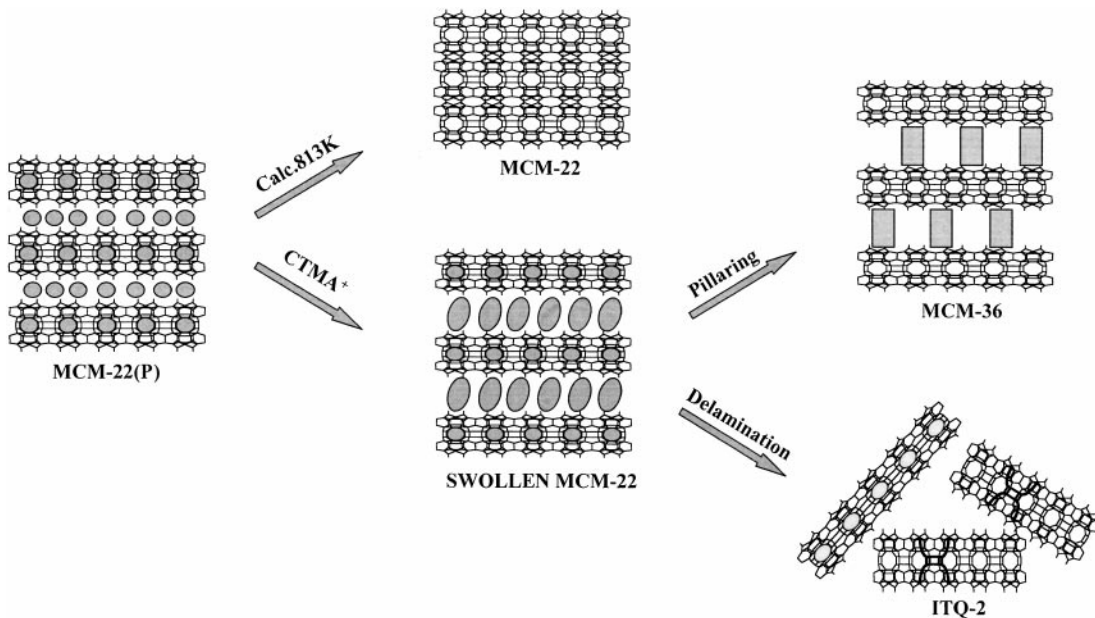


FIG. 1. Scheme for the preparation of the different materials obtained from the MCM-22 precursor.

molecules but it also has the handicap associated with the formation of coke on large cavities which are connected by small windows. In order to overcome these limitations, researchers from Mobil (20) have pillared the layered precursor and a new MCM-36 structure has been developed in which the 1.8×0.7 -nm cages are not closed but have the two halves separated by the pillars (see Fig. 1). However, despite the fact that the MCM-36 shows an increase in the external surface area, it also diminishes the number of acid sites at the actual external surface and, furthermore, it does not lead to the formation of pores (galleries) of regular size.

With the objective of preparing a material with a high and well structured external surface area we have followed a different approach which consists of delaminating the layered zeolite precursor of the MWW structure (21) in a way similar to that which can be done with clays. This allows large molecules access to active sites which would normally have been precluded by the size constraints imposed by the pore structure. We will show here that this procedure makes possible the preparation of a new material, called ITQ-2 (Fig. 1), formed by single layers organized in a "house of cards"-type structure, which is thermally stable and presents a well-defined and homogeneous external surface area of more than $700 \text{ m}^2 \text{ g}^{-1}$. This structure still presents zeolite characteristics, i.e., circular 10-MR channels, which makes ITQ-2 highly active and selective for processing large molecules.

In this paper, the physicochemical characteristics and catalytic behavior of ITQ-2 will be compared with those of MCM-22 and MCM-36, with the goal of understanding the catalytic implications of an active, well-defined, and homogeneous external surface area.

EXPERIMENTAL

Materials

The layered MCM-22 (*P*) precursor was prepared using hexamethylenimine (HMI) (Aldrich), silica (Aerosil 200, Degussa), sodium aluminate (56% Al_2O_3 , 37% Na_2O , Carlo Erba), sodium hydroxide (98% Prolabo), and deionized water. More specifically a sample with $\text{Si}/\text{Al} = 50$ was prepared in the following way. NaAlO_2 (0.234 g) and NaOH (0.816 g) were dissolved in 103.45 g of H_2O , and then, 6.358 g of HMI and 7.689 g of SiO_2 were added to this solution while stirring. After 30 min of stirring the resulting gel was introduced into a 60-ml PTFE lined stainless-steel autoclave, rotated at 60 rpm, and heated at 408 K for 11 days. The chemical composition of the final gel was $\text{SiO}_2/\text{Al}_2\text{O}_3 = 100$; $\text{OH}/\text{SiO}_2 = 0.10$; $\text{Na}/\text{SiO}_2 = 0.18$. After quenching the autoclaves in cold water, the samples were centrifuged at 12,000 rpm, washed thoroughly with deionized water until a pH of <9.0 was reached, and subsequently dried at $<333 \text{ K}$, overnight. A portion of this MCM-22 (*P*) was calcined in air at 853 K for 3 h giving MCM-22. Another portion was pillared with silica to form MCM-36, while a third portion was delaminated to generate the corresponding ITQ-2.

The pillarization process was carried out by mixing the swelled precursor with tetraethylorthosilicate (TEOS) in a 1:6 weight ratio. The mixture was heated at 353 K for 24 h under a N_2 atmosphere. The product was hydrolyzed in water for 5 h and then calcined in air at 853 K for 3 h, giving MCM-36 (20).

The ITQ-2 sample was obtained by swelling the precursor with hexadecyltrimethylammonium bromide. Typically,

27 g of precursor was mixed with 105 g of an aqueous solution of 29 wt% surfactant and 33 g of an aqueous solution of 40 wt% tetrapropylammonium hydroxide and refluxed for 16 h at 353 K. The completion of swelling can be monitored by X-ray diffraction (XRD), which shows an increase in the distance between the layers from 2.7 nm to approximately 4.5 nm. The layers are forced apart by placing the slurry in an ultrasound bath (50 W, 40 kHz) for 1 h. Subsequent addition of a few drops of concentrated hydrochloric acid, until the pH is below 2, allows harvesting of the solids by centrifuging. Then, removal of the organic material by calcination at 813 K yields ITQ-2 (22).

APPARATUS AND PROCEDURES

X-ray diffraction measurements were performed on a Philips X'PERT with automatic slits using $\text{CuK}\alpha$ radiation. IR spectra were obtained in a Nicolet 710 FTIR by using a Pyrex vacuum cell (CaF_2 windows) and self-supported wafers of 10 mg cm^{-2} . For acidity measurements, the samples were previously degassed at 673 K in vacuum (10^{-3} Pa) overnight (background spectrum). Then pyridine ($6 \times 10^2 \text{ Pa}$) was admitted at room temperature and degassed at 423, 523, and 673 K for 1 h. After each treatment spectra were recorded at room temperature and the background subtracted. Absorption isotherms of N_2 and Ar were obtained on an apparatus ASAP 2000 after pretreating the samples under vacuum at 673 K overnight.

n-Decane and vacuum gasoil (Table 1) were cracked, at 773 K, in a quartz fixed bed continuous reactor at atmospheric pressure. In all cases a given amount of feed was passed through the catalytic bed and the liquid products coming out from the reactor were condensed while the gaseous products were recovered in a gas buret by water displacement. After that, the reactor was purged with N_2 and the purged products were recovered in the liquid and gas receivers. In the next step, the catalyst was regenerated with air at 823 K for 3 h and the CO_2 and H_2O formed were measured to determine the coke on the catalyst. When the catalyst regeneration was completed, the system was purged with N_2 in order to remove the O_2 present. Then a new experiment with a new catalyst to oil ratio was started, since the catalyst remained stable after regeneration.

TABLE 1

Characteristics of Vacuum Gasoil

Density (g cc^{-1})	0.873	Conradson carbon (%wt)	0.03								
API gravity	30.6°	MeABP (°C)	366								
Nitrogen (ppm)	370	K-UOP	12.00								
Sulfur (ppm)	1.65	Viscosity (c.s. at 50°C)	8.249								
Distillation curve (°C)											
IBP	5	10	20	30	40	50	60	70	80	90	FBP
167	245	281	304	328	345	363	380	401	425	450	551

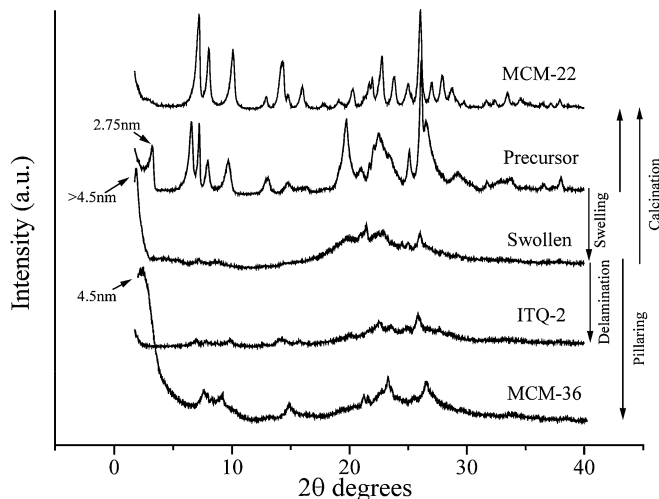


FIG. 2. X-ray diffraction patterns of the MCM-22 (*P*) and its derivatives.

The gas products were separated in a 15-m molecular sieve and a 50-m alumina-plot column and analyzed in TCD and FID gas-chromatography detectors. Liquids formed during the cracking of *n*-decane were separated in a 100-m Petrocol DH capillary column and analyzed in a FID detector. In the case of gasoil cracking, the liquids were analyzed by simulated distillation (ASTM, D-3907). More details on the reactor and the operational procedure can be found elsewhere (23).

RESULTS AND DISCUSSION

In Fig. 1 the different types of structures formed, starting from the laminar precursor, are schematized. It can be seen that while in the case of MCM-22 the large 1.8×0.7 -nm 12MR cavities are present, these should be absent in either MCM-36 or ITQ-2. Furthermore, it can also be seen that the external surface of individual layers of MWW structures leave half-open 12-MR cavities, which we call "cups," arranged in a regular array of approximately 0.7×0.7 -nm cups. By pillaring the precursor (see Fig. 1) one could increase the number of available cups since those pointing to the column gallery may also be accessible to reactants. However, one can see that, after pillaring, a large number of the open cups will also be covered by the pillars, preventing the accessibility of the reactants to the active sites located in those cups. A further look to Fig. 1 allow us to conclude that the highest possible amount of accessible cups will be obtained if a successful delamination of the laminar precursor was achieved.

We have recently shown this possibility (21) and followed the process by XRD (Fig. 2) by swelling the precursor with CTMA^+ . If the swelled material is pillared as described under Experimental, the XRD diagram corresponds to that reported for MCM-36. However, when the swelled precursor

was dispersed in water, as described under Experimental, it becomes delaminated and the resultant product (ITQ-2) appears almost amorphous to the X-ray. Indeed, ITQ-2 does not show the 00/ peaks with its 2.5-nm periodicity characteristic of a MWW topology. Comparing the XRD of ITQ-2 with that of a MWW-type zeolite, it can be seen that the high angle peaks are broader for ITQ-2, which is indicative of a reduction in the size of the crystal (domain of coherent scattering). In other words, delamination has significantly reduced the long-range order in the new material.

A high-resolution transmission electron microscopy (HRTEM) photograph allowed us to distinguish between the regular arrays of exposed 0.7×0.7 -nm cups and the 10-MR channel system in between them. Based on the proposed ITQ-2 structure simulations of the HRTEM image simulations were done using the Cerius Simulation Module, and they are consistent with the observed HRTEM image, thereby supporting the proposed ITQ-2 structure (21), which is schematically shown in Fig. 3.

The N_2 adsorption isotherms, shown in Fig. 4, are indicative of a progressive increase of total surface area and pore volume in the order $ITQ-2 > MCM-36 \gg MCM-22$, as can be seen in Table 2, where the values of total surface area and volume, as well as that of mesoporous (1.7 to 30 nm) area and volume, are summarized.

The Argon isotherms for MCM-22, MCM-36, and ITQ-2 clearly show (Fig. 5) that the three structures possess 0.5-nm-diameter micropores, corresponding to 10-MR channels, as observed by the absorption at low values of p/p_0 , but the amount of micropores is lower for MCM-36. The lower micropore volume of MCM-36 could be due to partial blocking of the 10-MR pores by silica. On the other hand, if one assumes that delamination has occurred, this

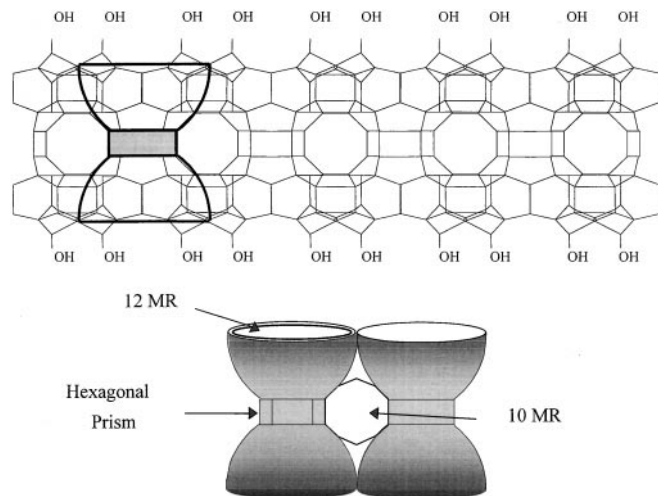


FIG. 3. Proposed structure for the ITQ-2 layer showing the characteristic 10-MR separating arrays of cups perpendicular to $\{00l\}$, with an artist impression of these cups included.

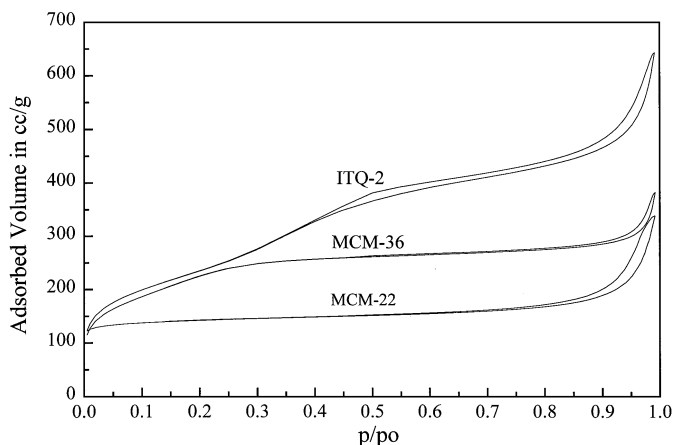


FIG. 4. Nitrogen adsorption isotherms of the different MCM-22 (P) derivatives.

will be consistent with the decrease some observed in the micropore volume of ITQ-2 with respect to that of MCM-22. Indeed, by delamination the large pore volume enclosed in the 1.8×0.7 -nm cavities disappears since, as can be seen in Fig. 1, delamination involves the disappearance of those cavities and the replacement by external “cups,” while the 10-MR circular channel still exists in the delaminated material. Argon isotherms in Fig. 5 confirms this assumption. Nevertheless the final microporosity observed is slightly lower than the one expected after delamination has occurred, indicating that some structure collapse has occurred during the delamination process.

From the Ar isotherm values, a Horvath–Kawazoe (25) type of representation has been performed and the results are given in Fig. 6. There can be seen not only in the presence of the micropores that still exist in MCM-36 and ITQ-2, but also in that, in the case of the MCM-36 structure, there is not a narrow regular array of pores within the pillar galleries as deduced by the extremely wide distribution of pore diameters in the 10- to 35-Å region.

The IR spectra of the MCM-22 and ITQ-2 are compared in the framework and hydroxyl vibration region (Fig. 7), and the results show that a larger number of SiOH groups

TABLE 2

Specific Surface Area and Volume of the Different Samples from Nitrogen Adsorption Isotherms

Sample	S_{total} ($m^2 g^{-1}$)	V_{total} ($cc g^{-1}$)	S_{meso} ($m^2 g^{-1}$) ^a	V_{meso} ($cc g^{-1}$) ^a
MCM-22	451	0.5239	96	0.1692
MCM-36	810	0.5920	458	0.3159
ITQ-2	841	0.9478	796	0.8533

^aCumulative desorption surface area and pore volume of pores between 1.7 and 30 nm in diameter, calculated using the BJH formalism (24).

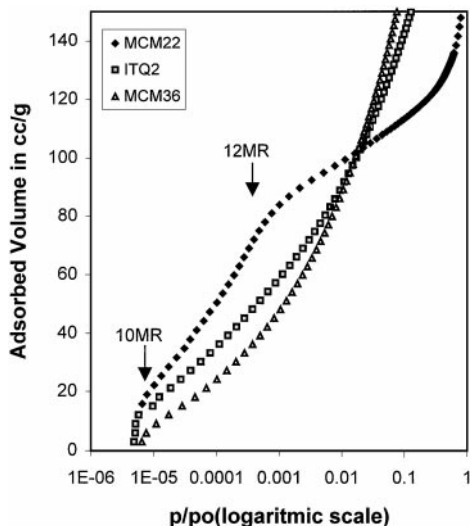


FIG. 5. Argon adsorption isotherms represented in a p/p_0 logarithmic scale to show the changes of slope corresponding to pore filling.

(bands at 3745 and 960 cm^{-1}) are present on ITQ-2, as it should be if a delamination of the layered precursor has occurred. Meanwhile, the spectroscopic results in the hydroxyl region shows that a decrease in the total number of acidic hydroxyl groups has occurred during delamination, probably due to the occurrence of a certain degree of dealumination. This should be reflected in the total number of Brønsted sites, as is indeed shown by the pyridine adsorption results (see Table 3).

It can be seen that a decrease in Brønsted acidity has occurred during delamination and pillarization, the decrease being much stronger for the pillared MCM-36 material. However, from the point of view of the cracking of large reactant molecules, the important parameter is not the to-

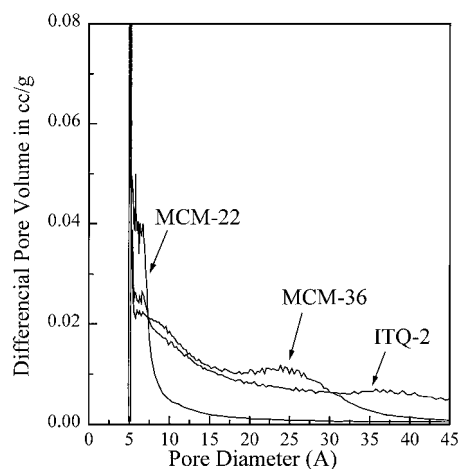


FIG. 6. Pore size distribution (Horwath-Kawazoe plot) for MCM-22, MCM-36, and ITQ-2.

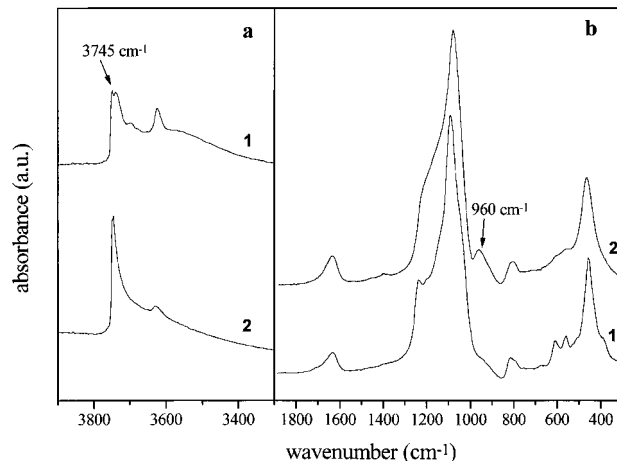


FIG. 7. Infrared spectra in the hydroxyl (a) and framework (b) range of the MCM-22 (1) and ITQ-2 (2).

tal Brønsted acidity but the number of acid sites accessible to the reactant. In order to discuss this, we have also carried out the adsorption of 2,6-ditertbutylpyridine (2,6-DTBPY) (spectra not shown) which certainly cannot enter into the circular 10-MR channels and, consequently, should only measure the amount of Brønsted acid sites accessible through the external surface, i.e., through the cups. When the acid sites measured with 2,6-DTBPY (26) are compared with the total number of acid sites as measured by the pyridine, it can be seen that a much larger number of external acid sites (~ 4 times higher) are present in ITQ-2 than in MCM-22. This again supports the hypothesis that delamination is increasing not only the external surface area but also the number of the Brønsted acid sites accessible to large molecules.

Catalytic Results

In order to carry out the catalytic evaluation of the above materials we have chosen two different feeds, *n*-decane and

TABLE 3

Acidity of the Different Samples Measured by Adsorption-Desorption of Pyridine at Increasing Temperatures and IR Spectroscopy

Samples	Acidity ($\mu\text{mol g}^{-1}$)		
	423 K	523 K	623 K
MCM-22 L	23	15	14
MCM-22 B	39	24	15
MCM-36 L	7	6	6
MCM-36 B	7	5	3
ITQ-2 L	23	20	15
ITQ-2 B	21	15	9

Note. Integrated molar extinction coefficients from Emeis (27).

a vacuum gasoil. The choice was made on the bases that *n*-decane can easily diffuse in all the pores of MCM-22, MCM-36, and ITQ-2 and therefore the *n*-decane cracking activity should be related with the total number of Brønsted acid sites present on these materials. On the other hand, most of the primary cracking of vacuum gasoil (Table 1) should occur only on the acid sites which are accessible through the external surface. Moreover, the different micropore volume present in the three structures should have an influence on the selectivity to the different products formed by consecutive reactions leading to re cracking, hydrogen transfer, and coke formation.

In Fig. 8, the *n*-decane cracking conversions measured at different catalyst to oil ratios, while keeping constant the

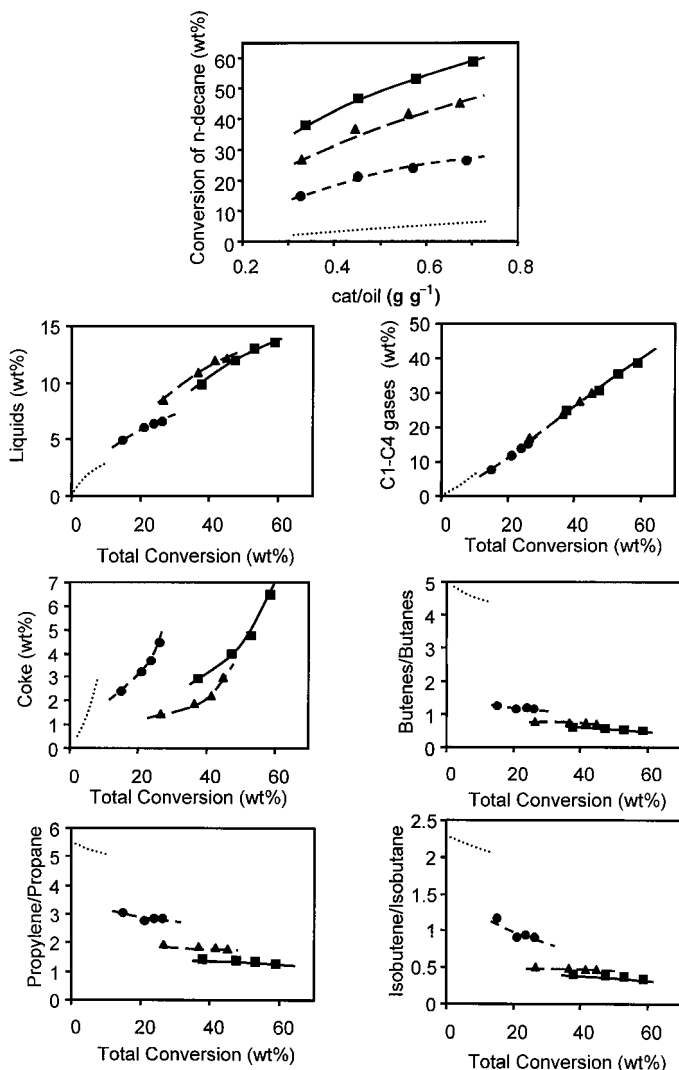


FIG. 8. Decane cracking. Conversion, selectivity curves, and ratio of olefins to paraffins in the gas products as a measure of the hydrogen transfer ability of (●) MCM-36, (■) MCM-22, (▲) ITQ-2, and (·) thermal cracking.

time on stream (TOS) at 60 s, have been plotted. It can be seen that the MCM-22 material, which contains the largest amount of Brønsted acid sites, is the most active cracking catalyst. This is followed by ITQ-2 and finally MCM-36, in agreement with the higher total acidity of the delaminated with respect to the pillared sample.

The influence of the larger proportion of acid sites in MCM-22 accessible through the 10-MR pores should make this catalyst more active for re cracking and, probably, more active for coke formation due to the presence of the large 12-MR cavities which are accessible only through 10-MR windows.

The results presented in the figure show that MCM-22 produces less liquids than either MCM-36 or ITQ-2. In the case of MCM-36, its much lower catalytic activity is responsible for the important contribution of the nonselective thermal cracking to the global conversion and selectivities observed, this being the probable reason for the higher amount of coke formed on MCM-36.

The extension of the hydrogen transfer can be taken into account by looking into the olefin/paraffin ratio in the C₃ and C₄ products and even better in the isobutene/isobutane ratio. The higher the ratio, the lower the extension to which hydrogen transfer reactions occur. Thus, it is that the C₃⁼/C₃ and C₄⁼/C₄ ratios are higher on MCM-36 than on ITQ-2 or MCM-22 owing to the absence, in the former, of the large 1.8 × 0.7-nm cavities present in MCM-22. Indeed, when large cavities are connected by relatively small pores, consecutive reactions, and even more so bimolecular reactions, are strongly enhanced. It is well known that, in the case of catalytic cracking, consecutive bimolecular reactions are responsible for hydrogen transfer and coke formation (14).

In the case of MCM-36, the contribution of thermal cracking to the overall activity is much more important than in the previous cases and this is responsible for the high olefinicity observed in the products. Moreover, consecutive reactions, such as hydrogen transfer, grow exponentially with the level of conversion. Taking all these considerations into account, the larger olefin/paraffin ratios observed on MCM-36 are not surprising.

In the case of gasoil cracking, the results given in Fig. 9 indicate that the order of activity is ITQ-2 ≫ MCM-36 > MCM-22, in agreement with the much higher amount of accessible acid sites present in the former. The higher ratio of “external” versus microporous surface in the case of MCM-36 and ITQ-2 is responsible for the formation of more liquids and less gases in the former two materials, ITQ-2 being more selective than MCM-36 for the formation of liquids. It is also worth pointing out that ITQ-2 produces less coke than either MCM-36 or MCM-22.

When looking into the ratios C₃⁼/C₃, C₄⁼/C₄, and iC₄⁼/iC₄, it is clear that both MCM-36 and ITQ-2 give a higher ratio of olefins to paraffins than MCM-22, showing a lower hydrogen transfer ability of the above structures. A closer

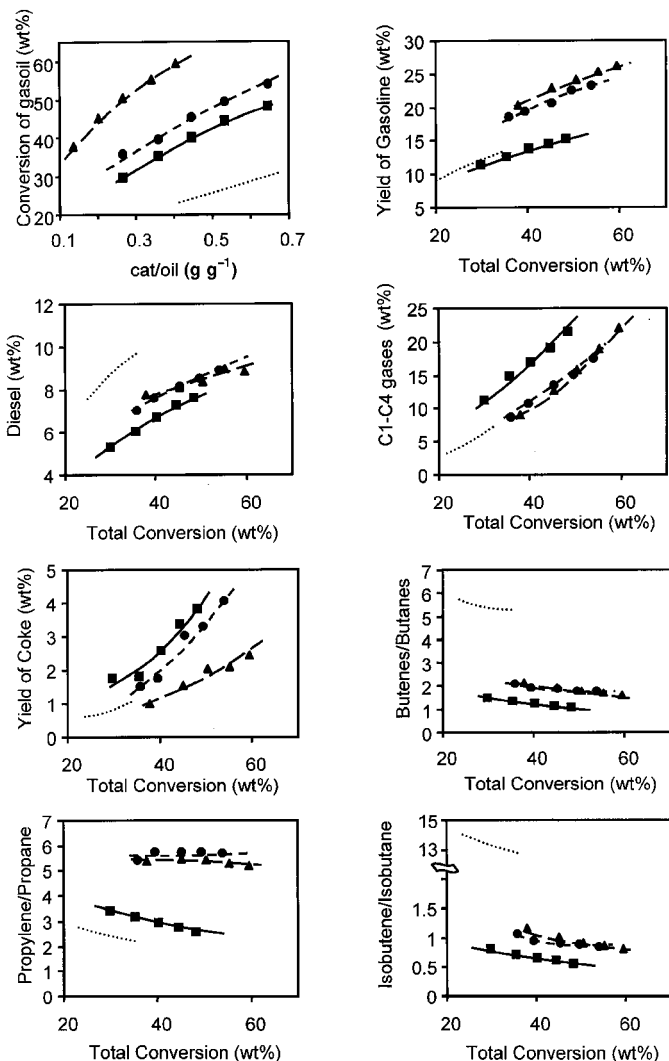


FIG. 9. Gasoil cracking. Conversion, selectivity curves, and ratio of olefins to paraffins in the gas products as a measure of the hydrogen transfer ability of (●) MCM-36, (■) MCM-22, (▲) ITQ-2, and (·) thermal cracking.

look to those figures, especially if the most sensitive isobutene/isobutane ratio is considered, shows that hydrogen transfer is even lower in ITQ-2.

CONCLUSIONS

The results presented here show the benefit of using ITQ-2 instead of MCM-22 or MCM-36 when large molecules are processed. This is due to the much higher well-defined external surface area, i.e., a larger number of cups present in the ITQ-2 structure, which in turn gives a larger amount of structurally accessible acid sites. The fact that ITQ-2 is stable during calcination at 550°C makes this material already interesting for acid catalyzed processes which do not require high regeneration temperatures, as is the

case for many oil refining, petrochemical, and chemical processes. In these cases, ITQ-2 can be of special interest since, owing to the absence of cavities or "long" pores, the diffusion of the products to the gas or liquid phase can quickly diminish the possibilities for the formation of bulkier consecutive products, with the corresponding benefit on selectivity and catalyst life.

ACKNOWLEDGMENT

We thank the Spanish CICYT for financial support (Project MAT97-0723 and Project MAT97-1207-C03-01).

REFERENCES

1. Corma, A., *Chem. Rev.* **95**, 559 (1995).
2. Zones, S. I., Olmstead, M. M., and Santilli, D. S., *J. Am. Chem. Soc.* **114**, 4195 (1992).
3. Zones, S. I., and Nakagawa, Y., US patent 407432, 1995.
4. Nakagawa, Y., and Zones, S. I., WO 96/29285, 1996.
5. Lewis, D. W., Willock, D. J., Catlow, C. R. A., Thomas, J. M., and Hutchings, G. J., *Nature* **382**, 604 (1996).
6. Lobo, R. F., Zones, S. I., and Davis, M. E., *J. Inclusion Phenom. Mol. Recogn. Chem.* **21**, 47 (1995).
7. Helmkamp, M. M., and Davis, M. E., *Annu. Rev. Mater. Sci.* **25**, 161 (1995).
8. Shanon, M. D., Casci, J. L., Cox, P. A., and Andrews, S. J., *Nature* **353**, 417 (1991).
9. Leonowicz, M. E., Lawton, J. A., and Rubin, M. K., *Science* **264**, 1910 (1994); Rubin, M. K., and Chu, P., US patent 4 954 325, 1990.
10. Casci, J. L., Cox, P. A., and Shannon, M. D., in "Proceedings, 9th International Zeolite Conference," p. 513, 1993.
11. Balkus, K. J., Jr., Gabrielov, A. G., and Saudler, N., *Mater. Res. Soc. Symp. Proc.* **368**, 359 (1995).
12. Wagner, P., Yoshikawa, M., Lovallo, M., Tsuji, K., Tasptsis, M., and Davis, M. E., *Chem. Commun.* 2179 (1997).
13. Martínez-Triguero, J., Díaz-Cabañas, M. J., Cambor, M. A., Fornés, V., Maesen, Th. L. M., and Corma, A., *J. Catal.*
14. Corma, A., Faraldos, M., Martínez, A., and Mifsud, A., *J. Catal.* **122**, 230 (1990).
15. Millar, D. M., and Garcés, J. M., PCT Int. Appl. WO 97/15528A1, 1997.
16. Fajula, F., in "Guidelines for Mastering the Properties of Molecular Sieves," NATO ASI Series B, Vol. 221, p. 53. Plenum Press, New York, 1990.
17. Corma, A., *Studies Surf. Sci. Catal.* **49**, 49 (1989).
18. Martens, J. A., Souverijns, W., Vettelst, W., Patton, R., Froment, G. F., and Jacobs, P. A., *Angew. Chem. Int. Ed. Engl.* **22**, 34 (1995).
19. Milini, R., Perego, G., Parker, W. O., Jr., Bellusi, G., and Carluccio, L., *Microsc. Mater.* **4**, 221 (1995).
20. Kresge, Ch. Th., Roth, W. J., Simmons, K. G., and Vartuli, J. C., WO patent 92/11934, 1992.
21. Corma, A., Fornés, V., Pergher, S. B., Maesen, Th. L. M., and Buglass, J. G., *Nature* **396**, 353 (1998).
22. Corma, A., Fornés, V., and Pergher, S. B., Patent 9605004EP, 1996, and WO 9717290, 1997.
23. Corma, A., and Martínez-Triguero, J., *J. Catal.* **165**, 102 (1997).
24. Barret, E. P., Joyner, L. G., and Halenda, P. P., *J. Am. Chem. Soc.* **73**, 373 (1951).
25. Horwath, G., and Kawazoe, K. J., *J. Chem. Eng. Jpn.* **16**, 470 (1983).
26. Corma, A., Fornés, V., Forni, L., Márquez, F., Martínez-Triguero, J., and Moscotti, D., *J. Catal.* **179**, 456 (1998).
27. Emeis, C. A., *J. Catal.* **141**, 347 (1993).